CHAPTER 8

Redox Signaling between DNA Repair Proteins for Efficient Lesion Detection: DNA Charge Transport within the Cell

Adapted from Boal, A. K., Genereux, J. C., Sontz, P. A., Gralnick, J. A., Newman, D. K., and Barton, J. K. (2008) (*submitted for publication*).

J. C. Genereux performed calculations. P. A. Sontz performed AFM experiments. J. A. Gralnick performed strain construction and aided in the design of genetics experiments.

INTRODUCTION

Base excision repair (BER) proteins, from bacteria to man, are challenged with combing the genome for DNA base lesions in order to maintain the integrity of our genetic material (*1-4*). This challenge is more remarkable to consider given the low copy number of these proteins and that they must discriminate among small differences between the modified and natural bases. In the case of MutY, a BER repair protein in *E.coli* with a human homolog, there are 30 proteins in the *E.coli* cell (*2*) to interrogate 4.6 million bases (*5*); the ratio of binding affinities for the target lesion, an 8-oxoguanine:adenine mismatch, versus well-matched native GC or AT base pairs is $\leq$ 1000 (*6*). Endonuclease III (EndoIII), another BER enzyme in the same protein family (*1-4*), recognizes a less prevalent lesion, hydroxylated pyrimidines, with equally low specificity; the copy number of EndoIII within *E.coli* is estimated as 500 (*2*). The enzymology has been well characterized regarding how MutY and EndoIII, as glycosylases, fix their substrate lesions once found (*1-4*), and the structures of MutY and EndoIII bound to DNA have been elucidated (*7, 8*), revealing the basis for substrate recognition. Yet how these lesions are efficiently detected remains to be determined.

Current models for genome scanning to detect lesions involve protein sliding along the DNA, squeezing the backbone, slipping bases out to allow for interrogation, or finding transiently opened sites (*9-13*). However, a simple sliding model, involving facilitated diffusion along the strand where each base is contacted and the interrogation is assumed to be instantaneous, yields a genome interrogation time, T, of 46 minutes for MutY, wholly insufficient given the doubling time in *E.coli* of 20 minutes. The time for sliding to scan the genome is calculated from a one-dimensional random walk (*9*). The one-dimensional diffusion (sliding) constant has been measured (*10*) *in vitro* for the DNA repair proteins hOGG1 and *Bacillus stearothermophilus* MutM as 5×10^6 bp^2/sec and

$3.5x10^5$ bp^2/sec respectively. Taking the more generous (faster) value for the diffusion constant, a genome size of $5x10^6$ base pairs, and the MutY copy number of 30 yields a scanning time of 46 minutes.

The higher copy number for EndoIII yields a significantly shorter interrogation time of 10 seconds for a much less prevalent lesion. These estimates for T significantly understate the problem, since the interrogation time cannot be instantaneous in the sliding model, and to slide along the strand, proteins, even water, must be displaced, which takes time. Some sliding models for facilitated movements of proteins along DNA incorporate hopping and intersegment transfer to locate a target (*9, 14*), but in a repair process, each base must be interrogated; hopping leads to an incomplete search.

DNA-mediated charge transport (CT) offers an alternative strategy to localize BER proteins in the vicinity of lesions. Ubiquitous to these low copy number BER proteins are [4Fe4S] clusters, common redox cofactors in proteins (*2-4*). While the mechanisms responsible for DNA CT chemistry are still being debated, it is now generally accepted that DNA-mediated CT can proceed over long molecular distances on a very short timescale (*15*). Oxidative damage to DNA has been demonstrated with oxidants covalently tethered and spatially separated from oxidized sites in the DNA duplex at distances of > 200 Å with negligible loss in efficiency (*16-18*). Previous studies have also established that CT through DNA is possible in biological environments that include nucleosomes (*19, 20*) and isolated HeLa cell nuclei (*21*). DNA CT is, however, extremely sensitive to perturbations in the intervening base pair stack (*22-24*). DNA mismatches, base lesions, and the binding of proteins that distort the DNA all serve to inhibit long range CT. Recently we have found that well-matched DNA covalently attached within a nanotube device can conduct charge through the π-stack

similarly to graphite through its π-stack, but the device resistance increases by 300-fold upon introduction of a single base mismatch (*25*). Given that this chemistry occurs at a distance and is modulated by the structural integrity of the base pair stack, we have considered that these reactions may be useful within the cell for long range signaling (*26-28*).

Our model for lesion detection involves cooperative DNA-mediated redox signaling among BER proteins containing [4Fe4S] clusters (Figure 8.1) (*26-28*). When not bound to DNA, these proteins are found in the $[4Fe4S]^{2+}$ state and are not easily oxidized or reduced under physiological conditions (*29*). The estimated potential for the $[4Fe4S]^{2+/1+}$ couple in EndoIII is -300 mV versus NHE while the potential for the $[4Fe4S]^{3+/2+}$ couple is estimated to be +250 mV versus NHE (*30*). Notably, the $[4Fe4S]^{3+}$ form of the protein is especially unstable in solution (*29, 30*). However, for MutY and EndoIII, we have demonstrated using DNA-modified electrodes that DNA binding shifts the 3+/2+ cluster potential more negative by > 200 mV (*26, 27, 30*); DNA-binding stabilizes the protein in the +3 form (*30*). Furthermore, the protein can be oxidized in a DNA-mediated reaction (*26, 27, 30, 31*). Thus we have proposed that these BER proteins bearing [4Fe4S] clusters exploit DNA-mediated CT as a very fast and sensitive method to detect damage inside the cell. As illustrated in Figure 8.1 (*b-d*), this DNA-mediated redox signaling model involves binding to DNA by one protein in the 2+ state (donor), which would promote electron transfer from the donor protein to a distal protein (acceptor), already bound to the helix and in the 3+ state. The donor protein is now oxidized and remains bound to DNA while the acceptor becomes reduced and diffuses away. Integral to this model is a differential DNA affinity for the $[4Fe4S]^{3+}$ and $[4Fe4S]^{2+}$ forms of the protein. In fact, the 200 mV potential

Figure 8.1. A model for DNA-mediated CT in DNA repair where DNA repair proteins, for example EndoIII (green) and MutY (orange), containing $[4Fe4S]^{2+}$ clusters bind DNA, activating them towards oxidation to the $[4Fe4S]^{3+}$ state. The sequence of events is as follows: Guanine radical formation can oxidize a repair protein in a DNA-mediated reaction, stabilizing the oxidized protein bound to DNA (*a*). A second protein binds in the vicinity of the first protein (*b, e*). Electron transfer to a distally bound protein can occur through the DNA p-stack if the intervening DNA is undamaged (*c, f*). The newly reduced protein has a diminished affinity for DNA and diffuses away (*d*). If, instead, a lesion site is present between the proteins (*g*), the DNA-mediated CT step is inhibited and the oxidized protein remains bound to DNA. In this search mechanism the sum of the DNA-mediated electron transfer steps between proteins constitutes a full search of the genome with the end result being a redistribution of low abundance DNA repair proteins in the vicinity of lesions.

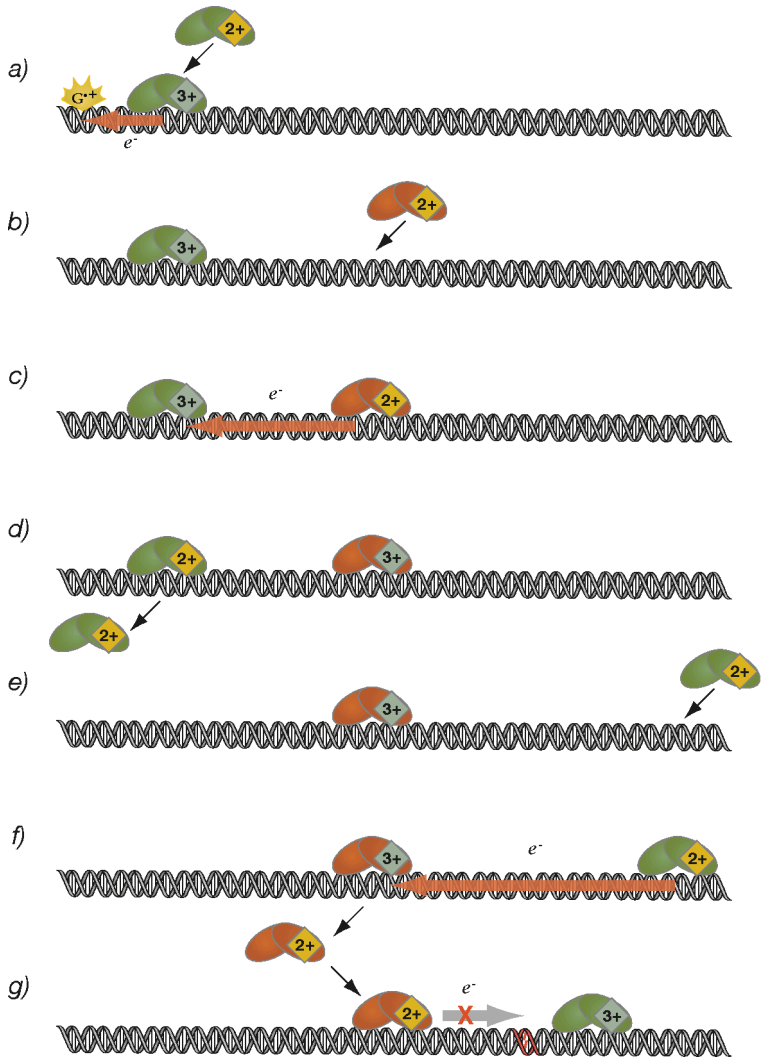

shift associated with DNA binding corresponds thermodynamically to a thousand-fold difference in DNA affinity between the oxidized and reduced proteins (*30*).

Importantly, this DNA-mediated CT process can be considered as a scan of the integrity of intervening DNA, since DNA-mediated CT can only proceed through a well stacked duplex. It should be noted that, although the DNA-mediated reduction occurs at potentials insufficient to damage the DNA (*32*), we have used a modified base to serve as a trap for the electron in this process and have found that binding of either MutY or EndoIII to the DNA promotes rapid reduction of the modified base (*31*). Thus DNA-mediated CT provides a means to distinguish whether the intervening DNA is intact or damaged. As illustrated in Figure 8.1 (*g*), when the repair protein, already oxidized, is bound in the vicinity of a base lesion, DNA-mediated CT does not provide a pathway for reduction and subsequent dissociation of the protein. The protein remains bound to the duplex so that on a slower timescale the protein can processively diffuse to the target site; now, however, sliding is needed only across a small region and the low specificity of the protein for its substrate (*33, 34*) is sufficient for recognition. Essentially, then, our proposal for base lesion detection based upon DNA CT involves redistributing the BER enzymes onto local regions of the genome that contain lesions. Critical to this mechanism is DNA-mediated signaling among proteins bound at long range so that the proteins, despite their low abundance, cooperate with one another in localizing onto target sites.

In order for the BER enzymes to exploit DNA-mediated CT to detect lesions, some of the proteins must exist in the oxidized state. Many agents in the cellular milieu could oxidize these DNA-bound proteins, and the level of oxidative stress within the cell could govern the proportion of oxidized protein present at any time. Indeed, these proteins can be oxidized by guanine radicals, the first genomic signal of oxidative stress (*35*), via DNA-

mediated CT. We have demonstrated the DNA-mediated oxidation of both MutY and p53, a cell cycle regulatory protein, with guanine radicals as intermediates (*28, 36*).

MATERIALS AND METHODS

Materials

All chemicals were purchased from Sigma Aldrich. All enzymes were purchased from New England Biolabs unless otherwise specified. All buffers were freshly prepared and filtered prior to use. Mica surfaces were purchased from SPI supplies. Silicon AFM probes were purchased from Nanoscience Instruments. Oligonucleotides were purchased from IDT or synthesized on a 3400 DNA synthesizer (ABI). All strains used were derivatives of CC104 or CC102 (*37*) and generated as described below. Luria-Bertani (LB) broth was used as the rich medium while NCE (*38*) medium supplemented with $MgSO_4$ (100 μM) and glucose (11 mM) or lactose (6 mM) was used as the minimal medium.

Generation of DNA Samples for AFM

Four primers were synthesized with the following sequences, 5'-GTACAGAGTTCAGTCGGCATCCGCTTACAGACAAGC-3' (forward), 5'-CCGGTAACTATCGTCTTGAGTCC-3' (reverse), 5'-GACTGAACTCTGTACCTGGCACGACAGGTTTCCCG-3' (forward), and 5'-GACTGAACTCTATACCTGGCACGACAGGTTTCCCG-3' (forward). The underlined bases highlight the location of a 2'-*O*-methyl residue. These primers were used in separate PCR reactions using pUC19 as a template to generate three duplexes 1610bp, 2157bp (matched), or 3767bp (mismatched) long and each containing one 14 nt single-

strand overhang. These PCR products were purified by ethanol precipitation and resuspended in 50 mM NaCl, 5mM sodium phosphate, pH 7 buffer and quantitated by OD_{260}. Duplexes were phosphorylated using 100 U PNK in 10% T4 DNA ligase buffer for 1 hour at 37°C and deactivated for 10 minutes at 65°C. Separate duplexes were then annealed at 65°C for 8 minutes then cooled to 20°C over 2 hours. The resulting larger duplexes were then ethanol precipitated and resuspended in 100 μL 50 mM NaCl/ 5mM phosphate buffer. 15 U T4 DNA ligase and 10% T4 ligase buffer were added (total reaction volume ~ 150 μL) and incubated overnight at 16°C followed by deactivation for 10 minutes at 65°C. We did not bring the ligation reaction to completion, so as to obtain a mixture of DNA samples that were equivalent other than the presence of the mismatch at the ligation site. The DNA duplexes (ligated and unligated) were then purified from a 0.6% agarose gel using a QiaQuick gel extraction kit (Qiagen).

AFM Deposition Conditions

Mica surfaces were freshly cleaved with scotch tape. Wild-type EndoIII (0.4 μM) was added to the stock DNA solution containing 50–100 ng total DNA composed of the mixture of ligated 3.8 kb duplexes and the two unligated duplexes (1.6 and 2.2 kb) in 6 mM $MgCl_2$/Tris-EDTA buffer. This protein-DNA solution was incubated at 4°C overnight and deposited (5 μL) on the mica surface for 2 minutes, rinsed with 2 mL water, and dried under argon. Two of the five wild-type EndoIII samples analyzed were deposited onto the mica surface in 5 ng quantities followed by immediate addition of 3.7 μM EndoIII (1 μL volume). This difference in deposition conditions did not result in any significant differences in the trends observed. Mutant protein (Y82A) was added to a stock solution

of 50 ng DNA for a final protein concentration of 0.4 μM. After incubation at 4°C overnight, deposition conditions were identical to that for wt EndoIII-DNA samples.

AFM Instrument Setup

Silicon AFM Probes purchased from Nanoscience Instruments (BudgetSensors), with a spring constant of 3 N/m and a resonance frequency of 75 kHz, were used in a Digital Instruments Multimode SPM. Images with scan areas of 2x2 μm^2 or 1x1 μm^2 were acquired in tapping mode, using an amplitude of 0.5416–0.200 V at a scan rate of 3.05 Hz. Scan rates of 3.05 Hz were used to obtain images of higher quality. Data analysis was performed using the WSxM program (*39*).

Strain Construction

CC104 and CC102 strains were generously donated (*37*), as was CC104 *mutY-* (CC104 *muty::*mini-tn 10) (*40*). *Nth* was replaced by a chloramphenicol resistance cassette (*cm*) in CC104 and CC104 *mutY-* using a previously described in-frame deletion method (*41*). See Table 8.1 for primer sequences; *nth* homology regions are shown in regular text and *cm* priming regions are highlighted in boldface. CC102 strains were constructed using P1 transduction (*42*). Inactivation in all strains was verified with colony PCR.

Lac^+ Reversion Assays

Strains were streaked to LB medium and incubated overnight at 37°C. For *nth* knockouts, strains were streaked to LB+chloramphenicol (17 μg/mL), and for *mutY* knockouts, strains were streaked to LB+tetracycline (50 μg/mL). 1 mL LB cultures were

Table 8.1. Primer sequences used for *nth* inactivation, cloning, and mutagenesis.

Function	Primer Sequence
Wanner inactivation of *nth*	5'-gaagcagctgcagaacgtgcattgccaaacggtgaaacagggaatgtctg**gtgtaggctggagctgcttc**-3'
	5'-agaggataaagaaaggttatcaatggggtaatcggtgttacccctttttct**catatgaatatcctccttag**-3'
Cloning *nth* into pBBR1MCS-4	5'-**ggaattc**gcaatggcacattgtttgac-3'
	5'-**aggttcc**tcaatggggtaatcggtgtt-3'
D138A mutant generation	5'-cggctggccgactattgctgtc**gcc**acgcacattttccgcg-3' + complement
Y82A mutant generation	5'-ggggtgaaaacctatatcaaaactattgggcttgctaacagcaaagc-3' + complement

started from single colonies and grown overnight in a shaking incubator at 37°C, 220 rpm. 20 μL of each starter culture was used to inoculate a 10 mL NCE+glucose culture which was then grown to a density of 10^9 cells/mL at 37°C, 250 rpm. Cell density was determined by dilution plating a 10 μL aliquot of the NCE+glucose culture onto NCE+glucose solid medium followed by incubation at 37°C for 36 hours. 5 mLs of this culture was centrifuged in a clinical tabletop centrifuge at 4°C and plated on NCE+lactose solid medium and then incubated at 37°C for 36 hours. Colonies arising are reported as *lac*$^+$ revertants/mL cells plated. In experiments incorporating plasmid vectors, CC104 and CC102 strains were made electrocompetent (*43*) and transformed via electroporation at 1.8 kV. Transformants were selected on LB+ampicillin (amp) (100 μg/mL) solid medium after incubation overnight at 37°C. Single colonies were restreaked to LB+amp (100 μg/mL) solid media and incubated 12 hours at 37°C. 1 mL LB+amp (100 μg/mL) cultures were started from these colonies and grown overnight at 37°C, 220 rpm. 20 μL of this starter culture was used to inoculate a 10 mL NCE+glucose+amp (40 μg/mL) culture which was grown to a density of 10^9 cells/mL at 37°C, 250 rpm. 5 mLs of this culture was plated onto NCE+lactose+amp (40 μg/mL) and incubated at 37°C for 36 hours. *Lac*$^+$ revertants were reported as described above.

Mutagenesis

Nth was cloned into pBBR1MCS-4 (p) using standard techniques (*43*). Primer sequences are given in Table S1; restriction sites are highlighted in boldface. Gene incorporation was verified by PCR and sequencing (Laragen) using KS/SK (pBBR1MCS-4 derived vectors) or M13 (pNTH10 derived vectors) sequencing primers. Mutants were generated using a QuikChange site-directed mutagenesis kit (Stratagene) and verified

by 3 independent sequencing reactions (Laragen). Primers used are shown in Table S1; the altered codon site is highlighted in boldface.

Protein Expression and Purification

EndoIII and Y82A EndoIII were expressed from the pNTH10 expression vector and purified as described previously (*44*). Protein concentrations were determined using the UV-visible absorbance of the [4Fe4S] cluster (410 nm, e = 17,000) (*29*).

Glycosylase Assays

Oligonucleotides were synthesized containing a 5-OH-dU lesion site (purchased as a phosphoramidite from Glen Research), HPLC purified, and verified with MALDI-TOF mass spectrometry. The following sequences were used: 5'-TGTCAATAGCAAGXGGAGAAGTCAATCGTGAGTCT-3' + complementary strand where X = 5-OH-dU base-paired with G. The strand containing the lesion was 5'-^{32}P endlabelled as previously described (*43*) and annealed to its complement. Reactions were run at 37°C for 15 minutes with 10 nM DNA and 100 or 10 nM protein and quenched with 1M NaOH (*45*). Samples were analyzed by denaturing 20% PAGE and imaged by autoradiography. Band intensity was quantified using ImageQuant software.

Electrochemistry at DNA-modified Electrodes

DNA-modified electrodes for protein electrochemistry experiments were prepared as described (*27*) using the following sequences: thiol-modified strand, 5'-AGTACAGTCATCGCG-3', TA complementary strand, 5'-CGCGATGACTGTACT-3', and abasic site (Ab) complementary strand, 5'-CGCGATGACTGTXCT-3', where X = dSpacer (Glen Research). Surfaces were backfilled with 100 mM mercaptohexanol for

30 minutes and rinsed at least 3 times with protein storage buffer (20 mM sodium phosphate, 100 mM NaCl, 0.5 mM EDTA, 20% glycerol, pH 7.5). Protein solution was introduced to the electrode surface and allowed to incubate for ~ 20 minutes until signal reached full intensity. Cyclic voltammetry experiments were performed on a CH Instruments 760 potentiostat using a 50 mV/s scan rate, Ag/AgCl reference electrode, and Pt wire auxiliary electrode in an electrochemical cell modified for protein experiments (*27*).

RESULTS AND DISSCUSSION

Genome Scanning Calculations

Using our CT scanning model, we can predict the genome interrogation time, T, for MutY in *E.coli*. In the CT scanning model, the DNA is essentially scanned by the electron with the repair proteins facilitating electron migration (Figure 8.1). Since an injected charge equilibrates on the nanosecond timescale (*15*), and protein diffusion occurs in micro- to milliseconds (*9*), the rate-limiting step in this process is the diffusion of a reduced protein within CT range of the oxidized DNA-bound protein. Hence scanning can be modeled as a random walk of the electron on the DNA, where the step time, *t*, for the walk is the average time for a reduced protein to approach within range to carry out DNA-mediated CT to the oxidized protein. We can calculate the step time for three dimensional diffusion of the reduced protein to the DNA as

$$t = \frac{V}{k_a C_p (1 - \Theta)}$$

where V is the cell volume, $C_p(1-\Theta)$ is the number of reduced repair proteins in the volume (Θ = fraction oxidized), and k_a is the bimolecular rate constant for protein association with the DNA target within the cellular volume. The bimolecular rate constant can be determined using a modified Smoluchowski equation for protein collision with a rod of DNA within the cell volume, where the length of the rod reflects the number of bases, *N*, over which DNA-mediated CT can proceed. The Smoluchowski equation is constructed with two terms: one describes the ballistic 3-dimensional diffusion of the protein to the DNA and the second (*46*) considers the gyrations of a rod with persistence length of 150 base pairs and the ends fixed as part of the chromosome.

$$k_a = 4\pi\kappa f D_p(r_{DNA} + r_p) + D_a a\sqrt[3]{\frac{r_{DNA} + r_p}{a}}$$

The protein diffusion constant (D_p) is determined from the Stokes-Einstein equation using the 10 cP viscosity of *E. coli* cytoplasm (*47*) and the measured Stokes radius of EndoIII (r_p) (*48*). DNA diffusion is considered to be negligible. The persistence length of DNA (150 bp) is defined as *a*. The electrostatic (*f*) and orientational (κ) constants are taken as unity (*49*), in keeping with the high ionic strength *in vivo* environment. The dissociation rate of the protein is not included in our model because charge equilibration should occur on a much faster timescale than dissociation of the reduced protein. Any contact of the reduced protein within the DNA rod allows electron transfer to the DNA-bound oxidized protein. We assume DNA is a rod, N base pairs long, but clearly the organization of the bacterial nucleoid is more complex (*50*). We can calculate the overall time to search the genome of *Z* bases through the random walk of the electron as

$$T_{ox} = t\left(\frac{4Z}{N}\right)^2$$

.

Since there is equal probability of reduced protein associating with each base in the CT-active target region, and N represents that maximum distance of interprotein charge transfer, the average distance of interprotein CT is N/2. Self-exchange decreases the average step distance by a further factor of 2. This represents the scanning time for a single oxidized protein. Each oxidized protein provides a separate nucleation site for CT scanning, but drawing from the same reservoir of reduced protein to scan different portions of the genome,

$$T_{CT} = t\left(\frac{4Z}{\Theta C_p N}\right)^2.$$

Scanning through sliding without a CT search represents a boundary condition, so that the total time is

$$T = (T_{CT}^{-1} + T_D^{-1})^{-1}$$

where T_D is the diffusion scanning time. It is also important to note that, since this model involves cooperation among the repair proteins, we can utilize the *total* concentration of these proteins within the cell, rather than copy numbers for MutY or EndoIII individually. Thus MutY benefits from help from the 500 copies of EndoIII (*2*).

This model assumes that DNA-mediated interprotein CT is much faster than protein diffusion, and that the oxidized repair proteins have higher nonspecific DNA affinity than the reduced proteins; both assumptions have experimental support (*15, 30*). We assume also that intervening DNA-binding proteins do not inhibit DNA-mediated CT, consistent with *in vivo* (*21*) and nucleosome (*19, 20*) experiments. We make no distinction between 5' to 3' versus 3' to 5' transport, although subtle differences have been observed (*51, 52*). In our model, reduced proteins are not allowed to exploit facilitated diffusion to find their DNA target containing oxidized protein, although this

would enhance the efficiency of the search. The possibility of other proteins participating in helper function, which would also substantially speed the search process, is neglected; other DNA-binding proteins at similar potentials could aid in helping MutY find its site (*53*). As formulated, there is an inverse cube dependence of scanning time on total copy number. Hence, the presence of even a hundred more redox-active repair proteins with this helper function would halve the overall scanning time. These conditions lead to an estimate for CT scanning that is conservative and therefore represents an overestimate for the amount of time necessary to search for lesions by DNA-mediated CT.

Figure 8.2 shows how the interrogation time varies as a function of N, the distance over which DNA-mediated CT proceeds and ox, the percentage of proteins that are oxidized. Remarkably, permitting DNA CT over 500 bp with 10% oxidized protein yields an interrogation time of 5 minutes, while DNA CT over only 200 bp with 20% oxidized protein results in an interrogation time of 8 minutes. These values are well within the 20 minute doubling time of *E. coli*. While we have not yet constructed long DNA sequences to establish the limits for long range DNA CT, we have demonstrated substantial long range oxidative damage in tethered DNA assemblies *in vitro* over 60 bp and in DNA within mitochondria over ~ 100 bp (*17, 54*). We and others have also found the distance dependence of CT to be remarkably shallow (*16-18, 55*). Long range CT has furthermore been demonstrated in nucleosomes with tethered photooxidants (*19, 20*). In fact, one advantage of DNA CT over other search mechanisms is that the electron travels *through* the DNA base pairs and no proteins need to be displaced.

The dependence of interrogation time on the percentage of proteins oxidized is also interesting to consider (Figure 8.2). There is a sharp decrease in the needed interrogation time at low levels of protein oxidized, and with higher oxidation levels the

Figure 8.2. Scanning time as a function of maximum distance of DNA-mediated interprotein CT (N) and the fraction of repair proteins that are in the 3+ state (% ox) is calculated using the CT scanning model. Note that at 10% oxidized protein with a maximum CT distance of 500 bp, the time required to interrogate the genome is ~ 5 minutes.

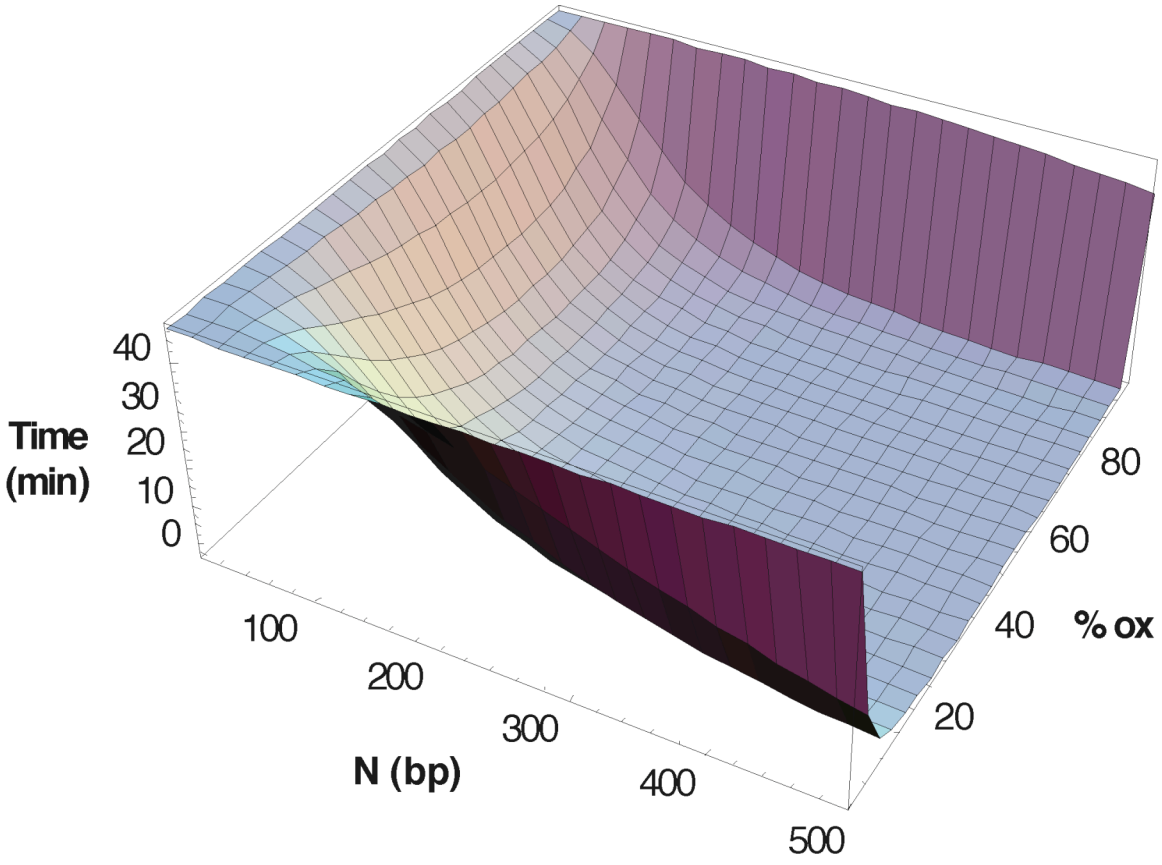

variation in interrogation time is quite small (Figure 8.3). The scanning efficiency resembles a switch that is turned on at low levels of oxidation, when DNA repair is needed. Activation of this switch could be influenced by the redox buffering capacity of the cell and by the level of oxidative DNA damage present. This would allow DNA repair proteins to sense oxidative assaults both locally and far away and to tune the repair response to fit the needs of the cell.

Atomic Force Microscopy Measurements

We can test this model directly using atomic force microscopy (AFM). A mixture of DNAs, both long (3.8 kilobase) DNA duplexes containing a single CA mismatch and short (2.2 and 1.6 kilobases) well-matched duplexes of the same total sequence were prepared; the longer sequence was obtained by ligation of the two shorter sequences. This mixture of matched and mismatched DNA strands was incubated with EndoIII and examined using established AFM techniques (*56*) (Figure 8.4). At least 5 images and > 100 strands were counted using 5 preparations of protein/DNA samples. We assume some adventitious oxidation of DNA-bound EndoIII, but have not yet carried out AFM measurements as a function of the percentage protein oxidized. The CA mismatch is a lesion that effectively inhibits DNA CT (*17, 23*). Since the CA mismatch is not a lesion that is preferentially bound by EndoIII, without DNA CT between bound EndoIII molecules, one might expect an equal density of proteins on the short and long strands. However, we find that EndoIII shows a small but significant preference for the longer strands containing the CA mismatch. Examination of the number of proteins bound to 187 long strands and 206 short strands reveals an average of 0.16±0.01 proteins bound per kilobase long strand and 0.12±0.02 proteins bound per kilobase short strand. Only clearly identifiable long or short strands were counted. Protein assignments were

Figure 8.3. Plot showing the contour from Figure 2 that corresponds to a genome scanning time (*T*) of 20 minutes, the doubling time of an *E. coli* cell.

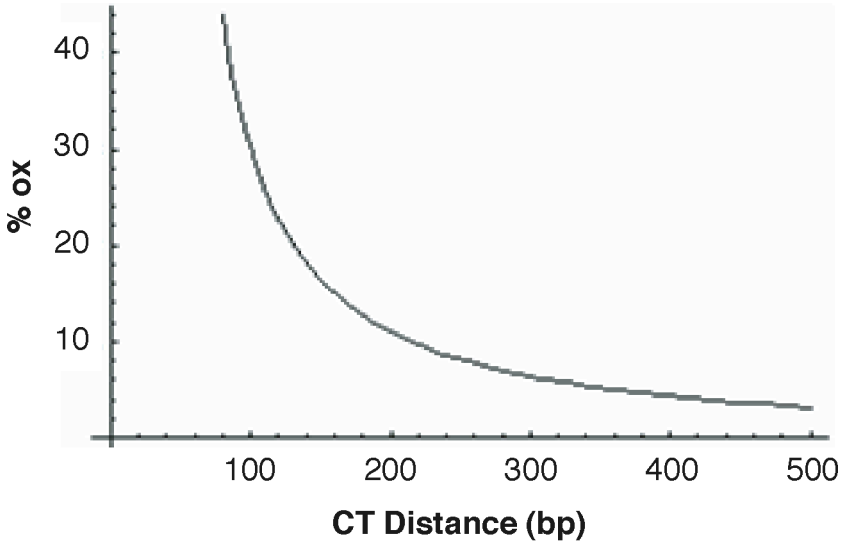

Figure 8.4. Measurements of repair protein distributions on DNA by AFM. A zoomed-in view (A) and a zoomed-out view (B) of representative AFM images of DNA strands incubated overnight with wild-type EndoIII. A higher density of proteins is apparent on the longer DNA strands containing the single base CA mismatch. Densities of 0.16±0.01 proteins bound per kilobase long strand and 0.12±0.02 proteins bound per kilobase short strand are observed where the error reflects the total number of bound proteins counted. Clumped DNAs and clumping at strand ends were excluded from the dataset.

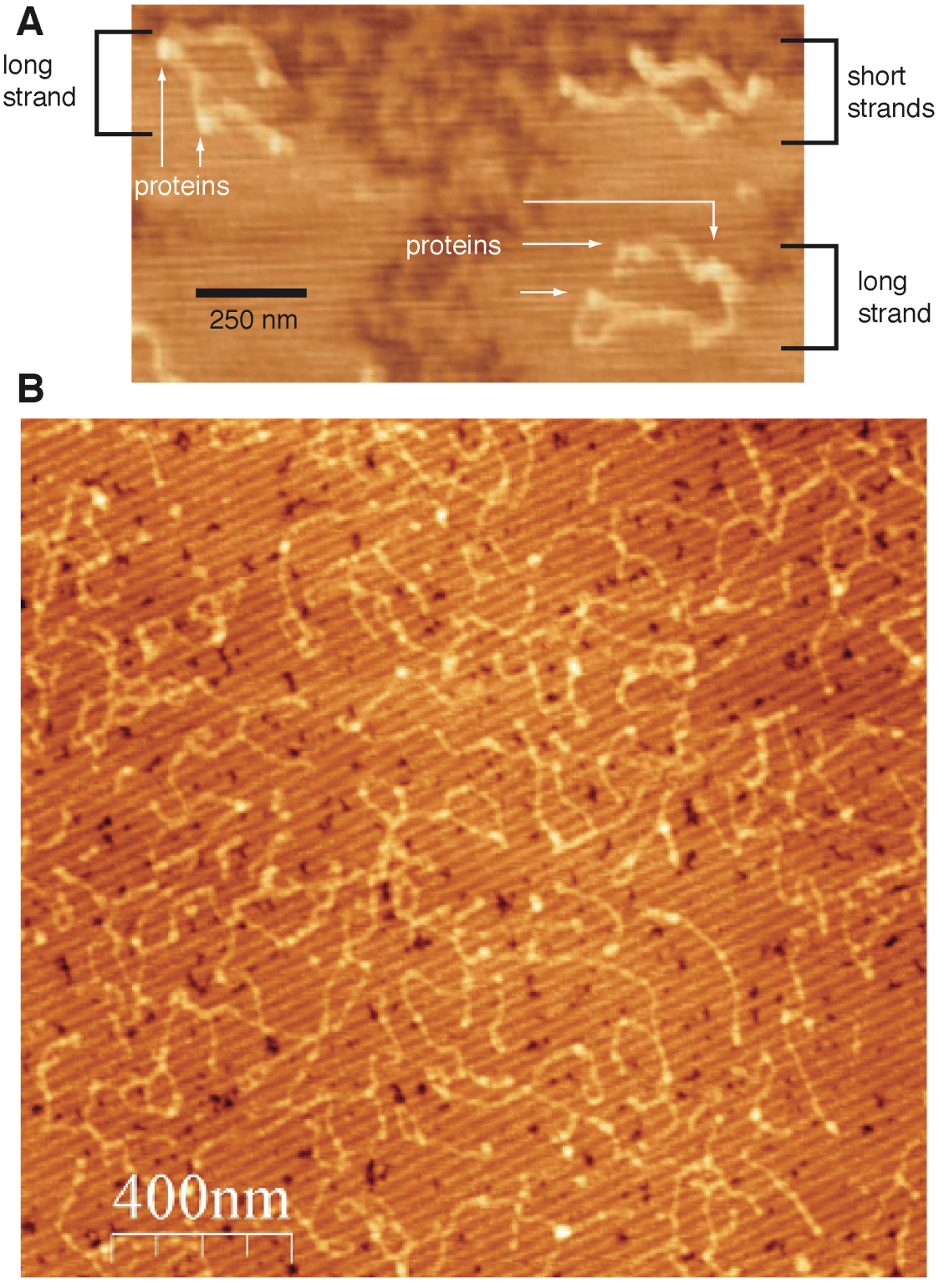

verified through analysis of their 4 nm heights in the images; without protein, features of this dimension are not observed. These results are consistent with the outcome predicted by our model. DNA-mediated CT will drive the redistribution of repair proteins away from undamaged regions such that the proteins will cluster near damaged sites. As a result, we see the proteins redistribute preferentially onto the DNA strand containing the mismatch.

Helper Function Assays in Escherichia coli

This CT scanning model can also be tested *in vivo* by assaying for the cooperation among the repair proteins in DNA-mediated signaling. If these proteins are able to help each other in their search for damage using DNA CT, upon knocking out the gene for EndoIII, for example, or reducing its capability to carry out electron transfer, one should be able to observe a decrease in the *in vivo* activity of MutY. Established assays for MutY and EndoIII activity inside *E. coli* cells have already been developed (*37*). The assay for "helper function" used here employs engineered mutations in the *lacZ* gene (encoding β-galactosidase, the enzyme that allows cells to grow in lactose-containing media) to report the frequency of a particular base pair substitution. The strain that serves as an assay for MutY activity, CC104, substitutes a cytosine for an adenine in the Glu 461 codon in *lacZ*, an amino acid essential for β-galactosidase activity. Since MutY prevents GC to TA transversion mutations (*57*), reversion of this original mutation back to wild-type (wt) *lacZ* can reflect a deficiency in MutY activity. Similarly, the CC102 strain serves as an assay for EndoIII activity by replacing an adenine with a guanine in the Glu 461 codon (*37*). EndoIII prevents GC to AT transition mutations (*58*); thus reversion back to wt *lacZ* indicates deficiency in EndoIII activity. In these experiments we

inactivated the gene encoding EndoIII (*nth*) in CC104, the MutY activity reporter strain, and looked for an increase in the reversion frequency from *lac-* to *lac+*. The reciprocal experiment, where the gene for MutY (*mutY*) is knocked out in the CC102 reporter strain, was also performed.

As illustrated in Table 8.2, in the CC104 MutY activity reporter strain, 20 ± 9 *lac+* revertants are observed per 10^9 cells, while inactivation of *mutY* in CC104 (CC104 *mutY-*) causes the number of *lac+* revertants to increase by a factor of 15 (300 ± 33), as expected (*37, 57*). When *nth* is inactivated in CC104 (CC104 *nth-*), the *lac+* reversion frequency observed is 54 ± 5, representing more than a factor of two increase over CC104. Thus, loss of EndoIII does have a small but significant effect on the *in vivo* activity of MutY. This loss in activity is consistent with a loss in helper function by EndoIII, as predicted by our model; the lower activity of MutY without EndoIII could reflect the lack of cooperative searching via DNA CT. An alternative explanation, however, is that MutY and EndoIII share some overlapping ability to repair the same lesions in genomic DNA. In this case, one would expect the *lac+* reversion frequency of the CC104 *mutY-/nth-* strain (270 ± 29) to be greater than that of CC104 *mutY-*, but they are, within error, equivalent.

We also performed the opposite experiment where *mutY* is inactivated and the resulting effect on the *in vivo* activity of EndoIII is observed using CC102, the EndoIII activity reporter strain (Table 8.2). An average of 14 ± 4 *lac+* revertants were found for the CC102 EndoIII activity reporter strain. Upon knocking out *nth* in CC102 (CC102 *nth-*), the reversion frequency becomes 34 ± 8. Removal of *mutY* (CC102 *mutY-*) leads to 27 ± 9 *lac+* revertants. In the double mutant (CC102 *nth-/mutY-*) 48 ± 16 revertants are observed. Note that the reversion frequency after inactivation of EndoIII is much

smaller for this assay than for the equivalent experiment (CC104 *mutY-*) using the MutY activity

Table 8.2. Assay for *in vivo* DNA repair by EndoIII (CC102) and MutY (CC104). *Lac+* revertants are reported as the average number *lac+* colonies that arise per 10^9 cells plated on minimal lactose media.

Strain	*lac*+ Revertants (*lac*+ colonies/ 10^9 cells plated)	Increase (x/CC104 or CC102)
CC104	20 ± 9	--
CC104 *nth-*	54 ± 5	2.7
CC104 *mutY-*	300 ± 33	15
CC104 *mutY-/nth-*	270 ± 29	13.5
CC102	14 ± 4	--
CC102 *mutY-*	27 ± 9	1.9
CC102 *nth-*	34 ± 8	2.4
CC102 *mutY-/nth-*	48 ± 16	3.4

assay and thus associated uncertainties are higher. In the CC102 assay, the mutagenesis pathway is likely initiated by damage to cytosine whereas in the CC104 assay the pathway likely begins with oxidative guanine damage. Given that the oxidation potential of guanine is substantially lower than that of cytosine, oxidized guanine lesions should be much more prevalent inside the cell (*35*), leading to a higher mutation frequency as observed with CC104. Nevertheless, the trend is the same: MutY appears to have a helper function in the EndoIII assay, just as EndoIII appears to have a helper function in the MutY assay. Indeed, just as the model predicts, MutY needs more help from EndoIII than *vice versa*.

This *in vivo* relationship between EndoIII and MutY has been observed previously by others, although in different experimental contexts. Small increases in mutational frequency have been detected when *mutY* is inactivated in CC102 (*37*) or when *nth* is inactivated in CC104 (*59*). In the latter case, it was proposed that this could be due to some intrinsic ability of EndoIII to repair oxidatively damaged guanine residues. However, biochemical evidence available on the substrate specificity of EndoIII (*34, 60*) indicates that the enzyme excises pyrimidine damage, which does not lead to GC to TA transversion mutations (*58*) and thus EndoIII would not be expected to exhibit MutY-like activity.

We can furthermore test directly whether the loss of MutY activity in the CC104 assay is the result of overlapping glycosylase activities by determining whether the number of *lac+* revertants is still suppressed by an EndoIII mutant that is biochemically incompetent to carry out the glycosylase reaction. As a control, we test for loss of EndoIII activity in the CC102 assay. Thus a mutant of EndoIII (D138A) that is known to be deficient in glycosylase activity (*61*) was introduced on a plasmid into both the CC102 and CC104 strains along with appropriate vector controls (an empty vector, p, and a

vector containing wt *nth*, pnth). Because this mutant cannot perform the base excision reaction, D138A also fails to reduce the high reversion frequency observed with CC102 *nth*- (Table 8.3). However, D138A is able to complement the CC104 *nth*- strain (Table 8.4). Thus, the glycosylase activity of EndoIII is not required to perform the helper function that EndoIII assumes to aid MutY in its repair of lesions inside the cell. Nonetheless, it appears that EndoIII lacking D138 can bind DNA and contains an intact [4Fe4S] cluster (*61*). Based upon our model, D138A should be competent to carry out DNA-mediated electron transfer and thus serve as a helper to MutY, as we observe.

In the context of our model, it is clearly not the glycosylase activity of EndoIII that is critical to its helper function, but its ability to carry out DNA-mediated CT. Thus, perturbing the path for electron transfer to the DNA would interfere with this helper function. Studies of protein electron transfer show that aromatic tyrosine and tryptophan residues often facilitate long range electron transfers in proteins (*62*), and EndoIII contains many of these residues. In particular, Y82 is a residue that is conserved in most species containing an *nth* homolog (in the human gene for EndoIII, *hNTH*, a W is present in this position, a relatively conservative substitution) as well as in many *mutY* homologs (*63*). In the crystal structure of *Bacillus stearothermophilus* EndoIII trapped in complex with DNA, the position equivalent to Y82 is located very close to the DNA backbone and directly adjacent to a residue that intercalates into the DNA base pair stack (*7*). Y82A EndoIII was thus introduced on a plasmid into both reporter strains (CC102 and CC104) and their *nth* knockouts to explore whether this mutation attenuates helper function. We find that Y82A is able to complement CC102 *nth*-. The observation that Y82A complements CC102 *nth*- further establishes that the glycosylase activity is not a source of helper function. Moreover the fact that Y82A complements CC102 *nth*- is understandable in the context of our model, because of the higher copy number of EndoIII in *E. coli* cells than MutY (*2*). MutY, therefore, is necessarily

Table 8.3. EndoIII activity assay (CC102) with an enzymatic EndoIII mutant (D138A). *Lac+* revertants are reported as the average number *lac+* colonies that arise per 10^9 cells plated on minimal lactose media with ampicillin (40 μg/mL). These data represent a single set of experiments with 10 replicates per strain assayed concurrently.

Strain	*lac*+ Revertants (*lac*+ colonies/ 10^9 cells plated)	Increase (x/CC102p)
CC102/p	10 ± 4.2	--
CC102 *nth-/p*	68 ± 26	6.8
CC102 *nth-*/pnth	18 ± 5.4	1.8
CC102 *nth-*/D138A	62 ± 31	6.2

Table 8.4. MutY activity assay (CC104) with an enzymatic EndoIII mutant (D138A). *Lac+* revertants are reported as the average number *lac+* colonies that arise per 10^9 cells plated on minimal lactose media with ampicillin (40 μg/mL). These data represent a single set of experiments with 10 replicates per strain assayed concurrently.

Strain	***lac*⁺ Revertants** (*lac*⁺ colonies/ 10^9 cells plated)	**Increase** (x/CC104p)
CC104/p	33 ± 2.0	--
CC104 *nth-/p*	64 ± 7.4	1.9
CC104 *nth-*/pnth	36 ± 3.3	1.1
CC104 *nth-*/D138A	32 ± 3.2	1.0

more dependent on a fast, efficient CT damage detection scheme to locate its lesions than EndoIII. In addition, oxidized guanine lesions, such as those excised by MutY, are much more abundant than the oxidized cytosine lesions repaired by EndoIII (*35*). Thus, the role of EndoIII in helping MutY search for lesions may more important than the ability of EndoIII to search for its own lesions.

Significantly, Y82A in the CC104 *nth-* strain shows an increase in mutation rate versus the CC104/Y82A and CC104/p controls (Figure 8.5). The data shown in Figure 8.5 is based on five sets of experiments with the CC104 strains. The number of *lac+* revertants is found to increase by 53±16% when comparing CC104 *nth-*/ Y82A to CC104/p. When comparing CC104 *nth-*/Y82A to CC104/Y82A, the number of *lac+* revertants increases by 68±13%. Similarly, for these trials, the ratio of the number of *lac+* revertants for CC104 *nth-*/ p versus CC104/p is 65±13%. If Y82A were attenuated but not completely defective in its electron transfer ability, we might expect that the number of *lac+* revertants measured in the CC104 assay would be lower on average for strains carrying this allele in the presence or absence of *nth* relative to their counterparts without it; this is what we observe (Figure 8.5). Together, these results indicate that Y82A is unable to restore helper function.

To check directly the biochemical characteristics of Y82A EndoIII, the protein was purified and its redox and glycosylase activities examined. Importantly, the mutant enzyme does contain the [4Fe4S] cluster, characterized by its distinctive spectrum with a maximum absorption at 410 nm (Figure 8.6). Y82A EndoIII also maintains glycosylase activity against a 5-OH-dU lesion in a ^{32}P-5'-endlabelled 35-mer duplex (Figure 8.7) as monitored by denaturing polyacrylamide gel electrophoresis; the activity of the mutant in this assay is equivalent (10% uncertainty) to that of the wild type enzyme. Note that this experiment on a 35-mer duplex measures only the base excision reaction, not the search process. To test for DNA-bound redox activity, Y82A was examined on a Au

Figure 8.5. Characterization of Y82A EndoIII, a mutant in DNA-mediated CT capability. Bar graph showing *lac+* revertants for CC102/p, CC102 *nth-*/p, CC102/Y82A, CC102 *nth-*/Y82A (left), CC104/p, CC104 *nth-*/p, CC104/Y82A, and CC104 *nth-*/Y82A strains (right). *Lac+* revertants are reported as the average number *lac+* colonies that arise per 10^9 cells plated on minimal lactose media containing ampicillin. Data for the CC104 strains are shown based upon five sets of independent biological experiments, each containing 10 replicates per strain. A statistically significant increase in the number of *lac+* revertants is observed in the CC104 *nth-*/Y82A strain (52±6) when compared to either the CC104/p (34±4) or the CC104/Y82A strain (31±2) indicating that Y82A does not restore helper function.

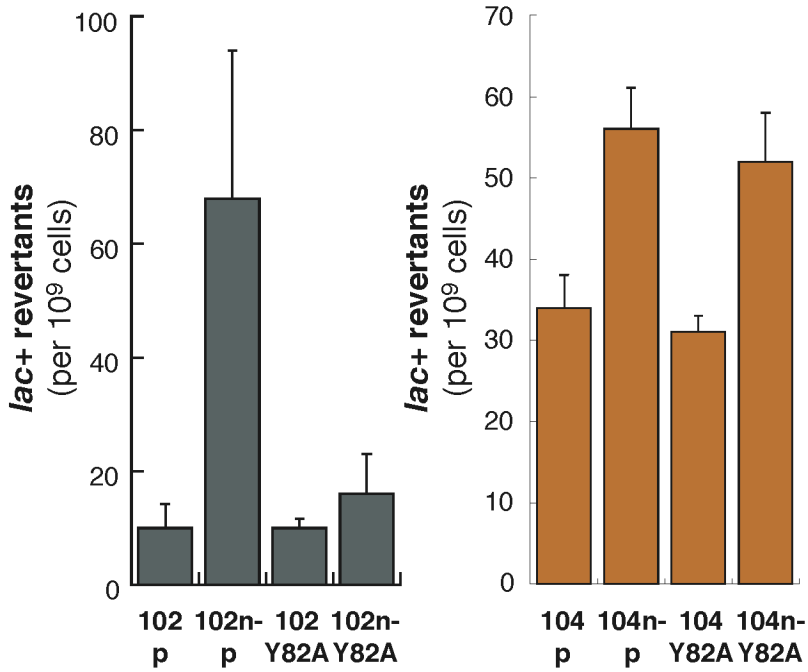

Figure 8.6. The UV-visible spectrum of Y82A EndoIII. A peak in the visible region is observed at 410 nm characteristic of a [4Fe4S] cluster.

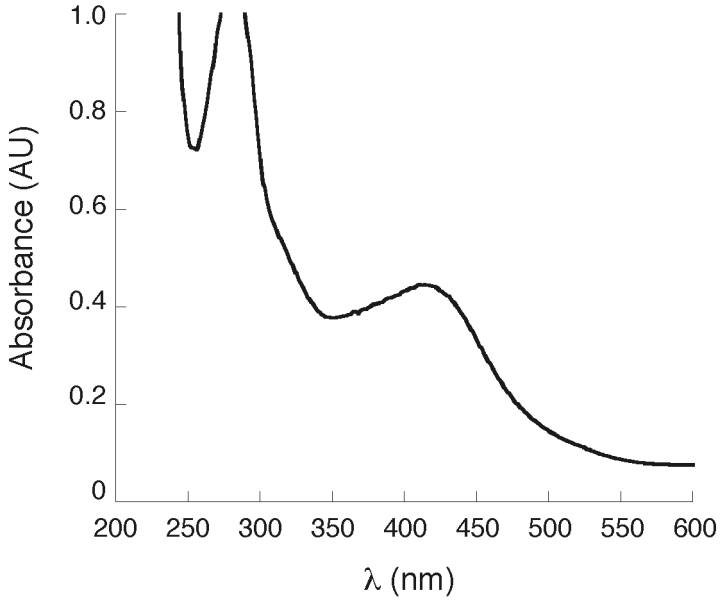

Figure 8.7. Autoradiogram after denaturing PAGE of ^{32}P-5'-TGTCAATAGCAAGXGGAGAAGT-CAATCGTGAGTCT-3' where X = 5-OH-dU base-paired with G. Protein samples (100 or 10 nM) were incubated with duplexes for 15 min at 37°C and quenched with 1 M NaOH. No significant difference in glycosylase activity is observed between Y82A and wt EndoIII.

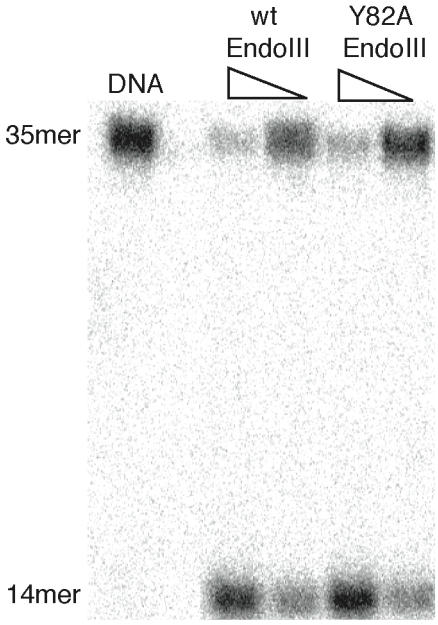

electrode surface modified with thiol-terminated DNA duplexes. Significantly, the potential for the DNA-bound mutant resembles that seen for the wild type protein (*27*), but the signal intensity is diminished (Figure 8.8). Note that, here, the protein concentrations are determined based on the 410 nm absorbance of the [4Fe4S] cluster; the smaller electrochemical signal observed with Y82A does not reflect a lower concentration of [4Fe4S] clusters. Over three trials, Y82A EndoIII exhibits a signal that is 50±13% smaller than that for wt EndoIII (per [4Fe4S] cluster). This lowered signal intensity would be expected with an attenuated efficiency of electron transfer from the cluster to the DNA. Y82A was also investigated at an electrode modified with a duplex containing an abasic site (Ab), a modification known to attenuate DNA-mediated CT to species bound above this lesion (*23*). Y82A does not exhibit a signal at this electrode modified with Ab (Figure 8.9) indicating that, as with wt EndoIII (*27, 30*), oxidation of the 4Fe4S cluster is DNA-mediated and requires an intact base pair stack. Significantly, and consistent with these results, examination of the distribution of Y82A on mismatched and matched strands by AFM shows no preference for the mismatched strand; 0.16±0.01 proteins per kilobase long strand and 0.18±0.02 proteins per kilobase short strand are observed (Figure 8.10). Thus Y82A not only is a mutant in “helper” function, but it also shows a compromised ability to carry out DNA-mediated CT. These results, considered together, demonstrate a distinct connection between DNA-mediated CT to the [4Fe4S] cluster and the *in vivo* relationship observed between MutY and EndoIII.

These experiments therefore indicate that MutY and EndoIII cooperate in their search for damage in the genome and redistribute in the vicinity of lesions consistent with our model for CT scanning. It is demonstrated that this cooperation, or helper function, does not involve the glycosylase reaction. Based on their chromosomal arrangement, the expression of MutY and EndoIII also do not appear to be linked (*64,*

Figure 8.8. Cyclic voltammetry of Y82A EndoIII at a Au electrode modified with $SH(CH_2)_2CONH(CH_2)_6NHOCO$-5'-AGTACAGTCATCGCG-3' + complementary strand. Scans were performed at 50 mV/s using a Ag/AgCl reference electrode and Pt wire auxiliary electrode. DNA-modified surfaces were prepared, backfilled with mercaptohexanol, and wt or Y82A EndoIII was tested. Surfaces were then rinsed and the other protein analyzed on the same surface. Over several trials, the electrochemical signal associated with Y82A is 50±13% smaller per [4Fe4S] cluster compared with wt EndoIII.

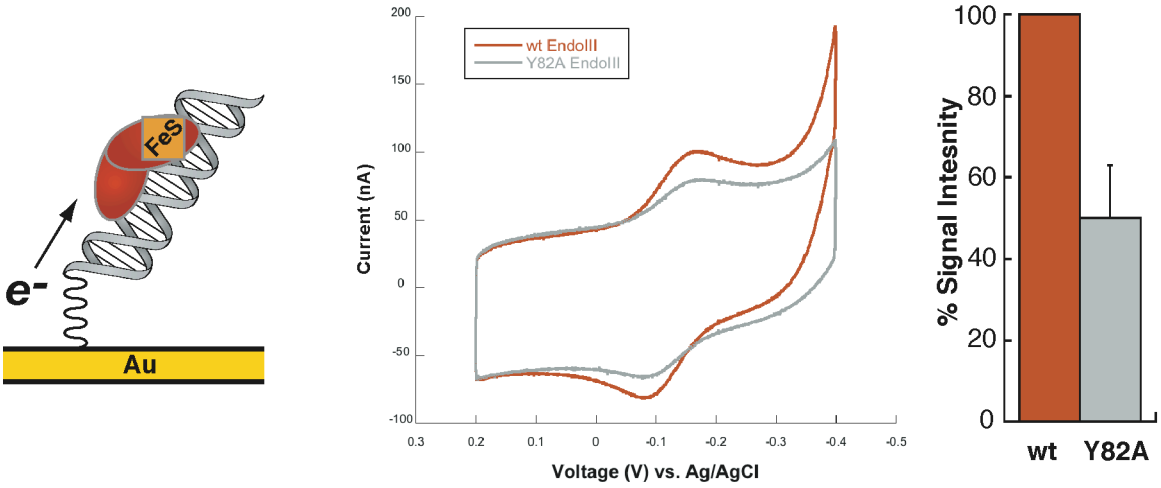

Figure 8.9. Y82A EndoIII examined by cyclic voltammetry at a Au electrode surface modified with DNA containing an abasic site. No peak is evident, indicating that CT to the [4Fe4S] cluster in Y82A EndoIII requires an intact DNA π-stack. See Materials and Methods section for further experimental details.

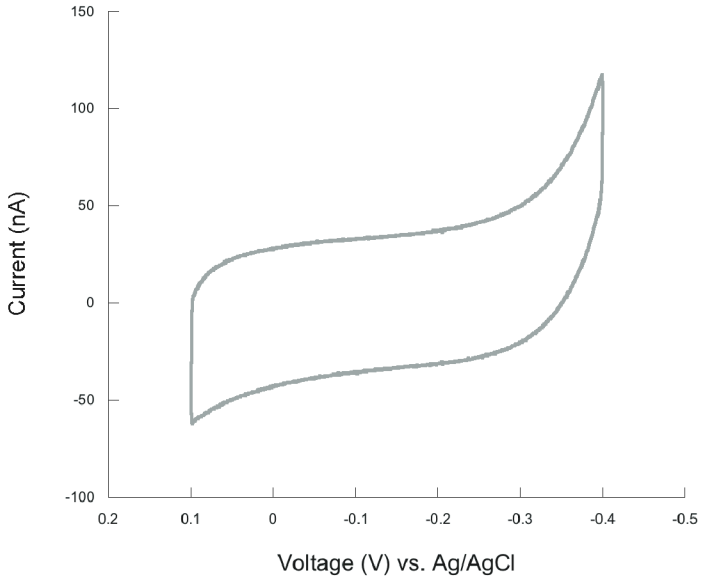

Figure 8.10. Comparative densities for wt (left) and Y82A (right) EndoIII bound to matched versus mismatched (CA) strands measured by AFM. Although wt EndoIII preferentially redistributes onto the mismatched strand, Y82A shows no preference.

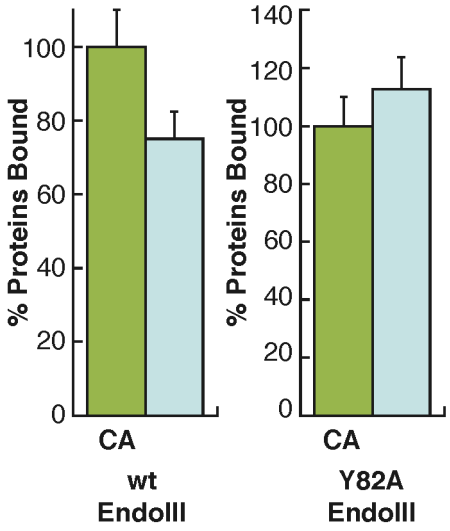

65). There is also no chemical evidence that the proteins physically bind to one another, and their low abundance within the cell makes random associations improbable. This cooperation thus arises from a distance. Importantly, what does appear to be required for helper function is an intact [4Fe4S] cluster, as well as an electroactive protein-DNA interface. Mutation of an aromatic amino acid residue near the DNA binding site, Y82A, leads to a decrease in CT efficiency *in vitro*, the inability of the protein to redistribute near lesions, and to diminished helper function *in vivo*. It is noteworthy that an analogous mutation (Y166S) in the human homolog of *mutY* is associated with cancer (*66*). While the detailed electron transfer pathway from this mutant to the DNA remains to be delineated, these experiments establish a link between DNA-mediated CT and the cooperative search for damage carried out by these repair proteins. These results thus provide biological support for our model of long range DNA-mediated signaling between repair proteins (Figure 8.1).

DNA-mediated CT chemistry serves as a fast and efficient reaction that is exquisitely sensitive to lesions and perturbations in the base pair stack. This chemistry helps to explain how these repair glycosylases locate their lesions efficiently in the cell, a key function since mutations in these enzymes in humans are implicated in colorectal cancer (*66*). This mechanism furthermore provides a rationale for iron-sulfur clusters in DNA repair proteins. More generally, these experiments illustrate the importance of DNA-mediated CT in long range signaling among proteins in low abundance that are bound to DNA. Other roles for DNA-mediated CT in biological signaling must now be considered.

SUMMARY

Given the remarkable sensitivity of DNA-mediated charge transport (CT) to mismatched and damaged base pairs, we have proposed that DNA repair glycosylases containing a redox active [4Fe4S] cluster (EndoIII and MutY) could use DNA CT in signaling one another to search cooperatively for damage in the genome. Here we examine this model for efficient CT scanning, where we estimate that electron transfers over a few hundred base pairs are sufficient for rapid interrogation of the full genome. Using atomic force microscopy, we find a redistribution of EndoIII onto DNA strands containing a single base mismatch, consistent with our model for CT scanning. We also demonstrate, using an *in vivo* assay for MutY activity in *Escherichia coli*, a cooperativity between EndoIII and MutY that is predicted by the CT scanning model. This helper function of EndoIII does not depend upon the enzymatic activity of the glycosylase but does depend upon its CT properties; Y82A EndoIII, a mutation that renders the protein deficient in DNA-mediated CT, as assayed with DNA electrochemistry, inhibits helper function. These results indicate a strategy for how these repair proteins efficiently locate DNA lesions and demonstrate a biological role for DNA-mediated CT within the cell.

REFERENCES

1. E. C. Friedberg, *et al.* (2006) *DNA Repair and Mutagenesis* ASM Press.

2. Demple, B., and Harrison, L. (1994) *Annu. Rev. Biochem. 63*, 915.

3. David, S. S., and Williams, S. D. (1998) *Chem. Rev. 98*, 1221.

4. David, S. S., O'Shea, V. L., and Kundu, S. (2007) *Nature 447,* 941.

5. Blattner, F. R., *et al.* (1997) *Science 277*, 1453.

6. Francis, A. W., Helquist, S. A., Kool, E. T., and David, S. S. (2003) *J. Am. Chem. Soc. 125,* 16235.

7. Fromme, J. C., and Verdine, G. L. (2003) *EMBO J. 22*, 3461.

8. Fromme, J. C., Banerjee, A., Huang, S. J., and Verdine, G. L. (2004) *Nature 427*, 652.

9. Berg, O. G., Winter, R. B., and von Hippel, P. H. (1981) *Biochemistry 20*, 6929.

10. Blainey, P. C., van Oijen, A. M., Banerjee, A., Verdine, G. L., and Xie, X. S. (2006) *Proc. Natl. Acad. Sci. U. S. A. 103*, 5752.

11. Parikh, S. S., *et al.* (1998) *EMBO J. 17*, 5214.

12. Wong, I., Lundquist, A. J., Bernards, A. S., and Mosbaugh, D. W. (2002) *J. Biol. Chem. 277*, 19424.

13. Parker, J. B., *et al.* (2007) *Nature 449*, 433.

14. Murugan, R. (2004) *Phys. Rev. E 69*, 011911 (2004).

15. Wagenknecht, H. A., Ed. (2005) *Charge Transfer in DNA: From Mechanism to Application,* Wiley-VCH.

16. Hall, D. B., Holmlin, R. E., and Barton, J. K. (1996) *Nature 382*, 731.

17. Nunez, M. E., Hall, D. B., and Barton, J. K. (1999) *Chem. Biol. 6,* 85.

18. Ly, D., Sanil, L., and Schuster, G. B. (1999) *J. Am. Chem. Soc. 121*, 9400.

19. Nunez, M. E., Noyes, K. T., and Barton, J. K. (2002) *Chem. Biol. 9*, 403.

20. Bjorklund, C. C., and Davis, W. B. (2006) *Nucleic Acids Res. 34,* 1836.

21. Nunez, M. E., Holmquist, G. P., and Barton, J. K. (2001) *Biochemistry 40*, 12465.

22. Boal, A. K., and Barton, J. K. (2005) *Bioconjug. Chem 16*, 312.

23. Boon, E. M., Salas, J. E., and Barton, J. K. (2002) *Nat. Biotechnol. 20,* 282.

24. Boon, E. M., Ceres, D. M., Drummond, T. G., Hill, M. G., and Barton, J. K. (2000) *Nat. Biotechnol. 18*, 1096.

25. Guo, X., Gorodetsky, A. A., Hone, J., Barton, J. K., and Nuckolls, C. (2008) *Nat. Nanotechnol. 3*, 163.

26. Boon, E. M., Livingston, A. L., Chmiel, N. H., David, S. S., and Barton, J. K. (2003) *Proc. Natl. Acad. Sci. U. S. A. 100*, 12543.

27. Boal, A. K. *et al.* (2005) *Biochemistry 44*, 8397.

28. Yavin, E., *et al.* (2005) *Proc. Natl. Acad. Sci. U. S. A. 102*, 3546.

29. Cunningham, R. P., *et al.* (1989) *Biochemistry 28*, 4450.

30. Gorodetsky, A. A., Boal, A. K., and Barton, J. K. (2006) *J. Am. Chem. Soc. 128*, 12082.

31. Yavin, E., Stemp, E. D. A., O'Shea, V. L., David, S. S., and Barton, J. K. (2006) *Proc. Natl, Acad. Sci. U. S. A. 103*, 3610.

32. Hickerson, R. P., Prat, F., Muller, J. G., Foote, C. S., and Burrows, C. J. (1999) *J. Am. Chem. Soc. 121*, 9423.

33. Porello, S. L., Leyes, A. E., and David, S. S. (1998) *Biochemistry 37*, 14756.

34. O'Handley, S., Scholes, C. P., and Cunningham, R. P. (1995) *Biochemistry 34*, 2528.

35. Burrows, C. J., and Muller, J. G. (1998) *Chem. Rev. 98*, 1109.

36. Augustyn, K. E., Merino, E. J., and Barton, J. K. (2007) *Proc. Natl. Acad. Sci. USA 104*, 18907.

37. Cupples, C. G., and Miller, J. H. (1989) *Proc. Natl. Acad. Sci. USA 86,* 5345.

38. Davis, R. W., Botstein, D., and Roth, J. R. (1980) *Advanced Bacterial Genetics: A Manual for Genetic Engineering* Cold Spring Harbor Laboratory.

39. Horcas, I., *et al.* (2007) *Rev. Sci. Instrum. 78*, 013705.

40. Golinelli, M. P., Chmiel, N. H., and David, S. S. (1999) *Biochemistry 38*, 6997.

41. Datsenko, K. A., and Wanner, B. L. (2000) *Proc. Natl. Acad. Sci. USA 97*, 6640.

42. Miller, J. H. (1992) *A Short Course in Bacterial Genetics: A Laboratory Manual and Handbook for Escherichia coli and Related Bacteria* Cold Spring Harbor Laboratory.

43. Sambrook, J., and Russell, D. W. (2001) *Molecular Cloning: A Laboratory Manual* Cold Spring Harbor Laboratory.

44. Boiteux, S., O'Connor, T. R., and Laval, J. (1987) *EMBO J. 6*, 3177.

45. Watanabe, T., Blaisdell, J. O., Wallace, S. S., and Bond, J. P. (2005) *J. Biol. Chem. 280*, 34378.

46. Berg, O. G. (1986) *Biopolymers 25*, 811.

47. Mullineaux, C. W., Nenninger, A., Ray, N., and Robinson, C. (2006) *J. Bacteriol. 188*, 3442.

48. Asahara, H., Wistort, P. M., Bank, J. F., Bakerian, R. H., Cunningham, R. P. (1989) *Biochemistry 28*, 4444.

49. Berg, O. G., and von Hippel, P. H. (1985) *Ann. Rev. Biophys. Chem. 14,* 131.

50. Thanbichler, M., Wang, S. C., and Shapiro, L. (2005) *J. Cell. Biochem. 96*, 506.

51. O'Neill, M. A., and Barton, J. K. (2002) *Proc. Natl. Acad. Sci. USA 99*, 16543.

52. O'Neill, M. A., Becker, H. C., Wan, C., Barton, J. K., and Zewail, A. H. (2003) *Angew. Chem. Int. Ed. 42*, 5896.

53. Gorodetsky, A. A., *et al.* (2008) *Proc. Natl. Acad. Sci. USA 105*, 3684.

54. Merino, E. J., and Barton, J. K. (2007) *Biochemistry 46*, 2805.

55. Kelley, S. O., Jackson, N. M., Hill, M. G., and Barton, J. K. (1999) *Angew. Chem. Int. Ed. 38*, 941.

56. Chen, L., Haushalter, K. A., Lieber, C. M., and Verdine, G. L. (2002) *Chem. Biol. 9*, 345.

57. Nghiem, Y., Cabrera, M., Cupples, C. G., and Miller, J. H. (1988) *Proc. Natl. Acad. Sci. USA 85*, 2709.

58. Kreutzer, D. A., and Essigmann, J. M. (1998) *Proc. Natl. Acad. Sci. USA 95*, 3578.

59. Tano, K., Iwamatsu, Y., Yasuhira, S., Utsumi, H., and Takimoto, K. (2001) *J. Radiat. Res. 42*, 409.

60. Dizdaroglu, M., Laval, J., and Boiteux, S. (1993) *Biochemistry 32*, 12105.

61. Thayer, M. M., Ahern, H., Xing, D., Cunningham, R. P., and Tainer, J. A. (1995) *EMBO J. 14*, 4108.

62. Stubbe, J., Nocera, D. G., Yee, C. S., and Chang, M. C. (2003) *Chem. Rev. 103*, 2167.

63. Watanabe, T., Blaisdell, J. O., Wallace, S. S., and Bond, J. P. (2005) *J. Biol. Chem. 280*, 34378.

64. Gifford, C. M., and Wallace, S. S. (2000) *Nucleic Acids Res. 28*, 762.

65. Gifford, C. M., and Wallace, S. S. (1999) *J. Bacteriol. 181*, 4223.

66. Cheadle, J. P., and Sampson, J. R. (2007) *DNA Repair 6*, 274.